




Rhesus Macaques Are More Susceptible to Progressive Tuberculosis than Cynomolgus Macaques: a Quantitative Comparison

Pauline Maiello,^a Robert M. DiFazio,^a Anthony M. Cadena,^a Mark A. Rodgers,^a Philana Ling Lin,^b Charles A. Scanga,^a  JoAnne L. Flynn^a

^aDepartment of Microbiology and Molecular Genetics, University of Pittsburgh School of Medicine, Pittsburgh, Pennsylvania, USA

^bDepartment of Pediatrics, Division of Infectious Diseases, UPMC Children's Hospital of Pittsburgh, Pittsburgh, Pennsylvania, USA

ABSTRACT In the past 2 decades, it has become increasingly clear that nonhuman primates, specifically macaques, are useful models for human tuberculosis (TB). Several macaque species have been used for TB studies, and questions remain about the similarities and differences in TB pathogenesis among macaque species, which can complicate decisions about the best species for a specific experiment. Here we provide a quantitative assessment, using serial positron emission tomography and computed tomography (PET-CT) imaging and precise quantitative determination of bacterial burdens of low-dose *Mycobacterium tuberculosis* infection in cynomolgus macaques of Chinese origin, rhesus macaques of Chinese origin, and Mauritian cynomolgus macaques. This comprehensive study demonstrates that there is substantial variability in the outcome of infection within and among species. Overall, rhesus macaques have higher rates of disease progression, more lung, lymph node, and extrapulmonary involvement, and higher bacterial burdens than Chinese cynomolgus macaques. The small cohort of Mauritian cynomolgus macaques assessed here indicates that this species is more similar to rhesus macaques than to Chinese cynomolgus macaques in terms of *M. tuberculosis* infection outcome. These data provide insights into the differences among species, providing valuable data to the field for assessing macaque studies of TB.

KEYWORDS *Mycobacterium*, PET CT, macaque, nonhuman primate, tuberculosis

Novel therapeutics for tuberculosis (TB) are greatly needed to curb the 10.4 million new cases and 1.8 million deaths that occur due to this global pandemic (1). Drugs have aided the fight against TB by saving an estimated 49 million lives between 2000 and 2015 (1). However, the current drug regimen is lengthy and cumbersome, and about 480,000 people developed multidrug-resistant TB in 2015 alone (1), so there is much room for improvement. The only licensed vaccine for TB, *Mycobacterium bovis* bacillus Calmette-Guérin (BCG), protects infants from severe manifestations of TB but does not provide long-lasting immunity against pulmonary TB (2). The urgent need for new therapeutics for TB has driven the development of novel drugs and vaccines that require preclinical evaluation in animal models. Many animal models are used in TB research, including mice, zebra fish, cattle, rabbits, guinea pigs, and nonhuman primates (NHPs) (3, 4). Mice and NHPs are the two animal models that are the most useful, as the other models suffer from a lack of resources available for immunologic studies. Mice have their shortcomings too, as their TB pathology is not fully representative of the pathology observed in humans, and they do not develop human-like latent TB infection (LTBI). NHPs recapitulate the full spectrum of *Mycobacterium tuberculosis*

Received 17 July 2017 Returned for modification 15 August 2017 Accepted 19 September 2017

Accepted manuscript posted online 25 September 2017

Citation Maiello P, DiFazio RM, Cadena AM, Rodgers MA, Lin PL, Scanga CA, Flynn JL. 2018. Rhesus macaques are more susceptible to progressive tuberculosis than cynomolgus macaques: a quantitative comparison. *Infect Immun* 86:e00505-17. <https://doi.org/10.1128/IAI.00505-17>.

Editor Sabine Ehrh, Weill Cornell Medical College

Copyright © 2018 American Society for Microbiology. All Rights Reserved.

Address correspondence to Charles A. Scanga, scangaca@pitt.edu, or JoAnne L. Flynn, joanne@pitt.edu.

P.L.L., C.A.S., and J.L.F. contributed equally to this article.

For a commentary on this article, see <https://doi.org/10.1128/IAI.00776-17>.

infection and pathology seen in humans (5–8). Immunologic reagents for NHPs are readily available, and tissue-based studies can be performed on NHPs that are not possible in humans (reviewed in reference 8).

NHPs have been reported by our research group and others to reflect key aspects of human disease, such as clinical latency, granuloma structure, and range of pathologies (5–8). TB studies were first explored with rhesus macaques (*Macaca mulatta*) in the 1970s (9, 10). However, the cynomolgus macaque (*Macaca fascicularis*) was the first to demonstrate evidence of LTBI after low-dose *M. tuberculosis* infection (11). Our laboratory further characterized this model and has since developed it extensively. We demonstrated that in cynomolgus macaques infected via a bronchoscope with a low-dose Erdman strain of *M. tuberculosis*, approximately 50% had active progressive disease (5) using clinical signs such as *M. tuberculosis* growth from gastric aspirate (GA) or bronchoalveolar lavage (BAL) fluid samples (12) and increased erythrocyte sedimentation rate (ESR) (13), as well as chest radiographs. The other half of the macaques had no signs of disease in the 15 to 20 months of the study and were clinically latent. Subsequent studies demonstrated that this cynomolgus macaque model recapitulated the full spectrum of TB encompassing both active disease and latent infection (LTBI) (6). Furthermore, monkeys with LTBI could be reactivated following anti-tumor necrosis factor (anti-TNF) treatment (14), CD4 T cell depletion (15), or simian immunodeficiency virus (SIV) coinfection (16). The Erdman strain has also been used in rhesus and cynomolgus macaques by other research groups (17–21), and a comparison of BCG vaccination followed by high-dose *M. tuberculosis* strain Erdman challenge in these two species suggested that cynomolgus macaques had improved control of infection (22). There is evidence for LTBI in rhesus macaques using the H37Rv strain delivered at a low dose (23) or the less virulent strain CDC1551 strain delivered at higher doses and reactivation of CDC1551 LTBI by SIV (24). The route of challenge (aerosol versus bronchoscopic challenge) in rhesus macaques influences the distribution of disease but not the overall outcome of the infection (25). We have used Chinese cynomolgus macaques (CCM) to demonstrate that most granulomas form from a single bacterium and that individual granulomas follow distinct trajectories even within the same host (26), highlighting the importance of local immune control in influencing host outcome (27). Importantly, the full range of granuloma types (e.g., caseous, nonnecrotic, fibrotic, etc.) and pathologies (e.g., cavities, consolidations, and TB pneumonia) can be observed in *M. tuberculosis*-infected macaques (7). Thus, the NHP models have been useful for basic studies on immunology and pathogenesis, as well as for testing drugs and vaccines (reviewed in reference 8).

Medical imaging has been used in NHPs for tracking disease using a variety of modalities (21, 28). We use serial positron emission tomography and computed tomography (PET-CT), which combines a functional map (PET) of the thoracic cavity, depending on the PET probe used, with a spatial map of anatomic structures (CT) (29). Using this imaging strategy in our macaques, we can assess drug efficacy *in vivo* (29, 30) and study critical events during infection (26, 31–33). Comparative genomic studies have been performed for rhesus and cynomolgus macaques and showed that, while abundant heterogeneity exists in each population, there is an extraordinarily high degree of similarity in both species to human genes (34), and there is great similarity in the T cell responses to *M. tuberculosis* epitopes between both cynomolgus and rhesus macaques and humans (35). There are data that rhesus macaques are more susceptible than cynomolgus macaques following aerosol challenge, but this study lacked quantitative bacterial burden data and consisted of relatively small numbers of animals (19). Mauritian cynomolgus macaques (MCM) represent a newer potential model system. MCM originate from the island of Mauritius, and they have limited major histocompatibility complex diversity due to extreme founder effects that created a tight genetic bottleneck (36). Aerosol challenge with *M. tuberculosis* has been described in these animals (21, 37), and they appeared to be quite susceptible to TB.

The goal of this study was to provide a quantitative comparison of three NHP species that are potential models for preclinical evaluation of novel TB therapeutics and

TABLE 1 Clinical measures by species^a

Clinical measure	% of macaques (n)		
	CCM (n = 26)	Rhesus (n = 18)	MCM (n = 6)
Coughing ^b	19.2 (5)	66.7 (12)	33.3 (2)
ESR of ≥5 mm/h	53.9 (14)	61.1 (11)	16.7 (1)
CFU+ GA or BAL (>60 days p.i.)	46.2 (12)	72.2 (13)	33.3 (2)
Humane euthanasia endpoint ^c	15.4 (4)	38.9 (7)	66.7 (4)

^aCough, erythrocyte sedimentation rate (ESR) of at least 5 mm/h at any time postinfection, and *M. tuberculosis* growth (CFU represents colony-forming units) from gastric aspirate (GA) samples or bronchoalveolar lavage (BAL) fluid samples after 60 days postinfection were recorded for each animal in the study, and percentage of positive macaques for each species is shown. The percentages of each species that had early necropsies (humane euthanasia endpoint) due to clinical concerns are displayed here. The Fisher exact test was used to compare CCM and rhesus macaques only.

^b*P* < 0.01.

^c*P* = 0.0926.

vaccines: CCM, MCM, and rhesus macaques. These macaques received the same strain of *M. tuberculosis* (Erdman) through the same route of inoculation and were monitored using similar clinical, microbiologic, and imaging methods (PET-CT). All macaques had detailed necropsies. The data from this study highlight similarities and differences in *M. tuberculosis* infection outcomes among these different NHP species, as well as the variability within each single species.

RESULTS

Rhesus macaques display more clinical signs of disease than cynomolgus macaques do. Our goal was to investigate differences in *M. tuberculosis* infection outcomes in two macaque species. Chinese cynomolgus macaques (CCM) (*n* = 26) and Chinese rhesus macaques (*n* = 18) enrolled in a series of different studies in our laboratories were infected with low-dose *M. tuberculosis* strain Erdman via bronchoscopic instillation into a lower lung lobe. These macaques were subjected to serial PET-CT scans and clinical and microbiologic monitoring and necropsied between 2 and 6 months postinfection (see Table S1 in the supplemental material). We also had the opportunity to compare these macaques to a more limited number of Mauritian cynomolgus macaques (MCM) (*n* = 6) that were infected and monitored similarly.

CCM, as we previously reported (5, 6), have a large range of outcomes following low-dose infection; clinically, they present across a spectrum from what is known as latent TB (LTBI) to severe active TB. There are several clinical criteria for TB disease that we and others have previously used in macaques, including the erythrocyte sedimentation rate (ESR) or C-reactive protein—both nonspecific measures of inflammation, *M. tuberculosis* growth from bronchoalveolar lavage (BAL) fluid or gastric aspirate (GA) samples, weight change, cough, and clinical indications for humane euthanasia (which can include increased respiratory rate or effort, poor appetite, and deterioration in general physical condition). In our previous work, we reported approximately equal proportions of latent or active *M. tuberculosis* infection in CCM following low-dose infection, using the criteria for active TB of a positive *M. tuberculosis* culture after 60 days and presence of any clinical signs, including persistently elevated ESR (5, 6). By clinical measures (Table 1), rhesus macaques in the current study developed more progressive TB disease than CCM. Coughing was reported in 66% (12/18) of rhesus macaques compared to 19% (5/26) of CCM (*P* = 0.0038 by Fisher's exact test). A maximum ESR of ≥5 mm/h was recorded for 61% (11/18) of rhesus macaques and 54% (14/26) of CCM but only 17% (1/6) of MCM. GA and/or BAL fluid sampling were performed monthly, and *M. tuberculosis* growth was determined. In our previous studies, we found that CCM can have culture-positive BAL fluid or GA samples early postchallenge (<60 days postinfection[p.i.]) but that they do not necessarily progress to active TB, while positive cultures after 60 days p.i. are associated with active TB (6). In this study, 72% of rhesus macaques had a positive GA or BAL fluid sample after 60 days of infection, while 46% of CCM did (*P* = 0.1245 by Fisher's exact test). Although

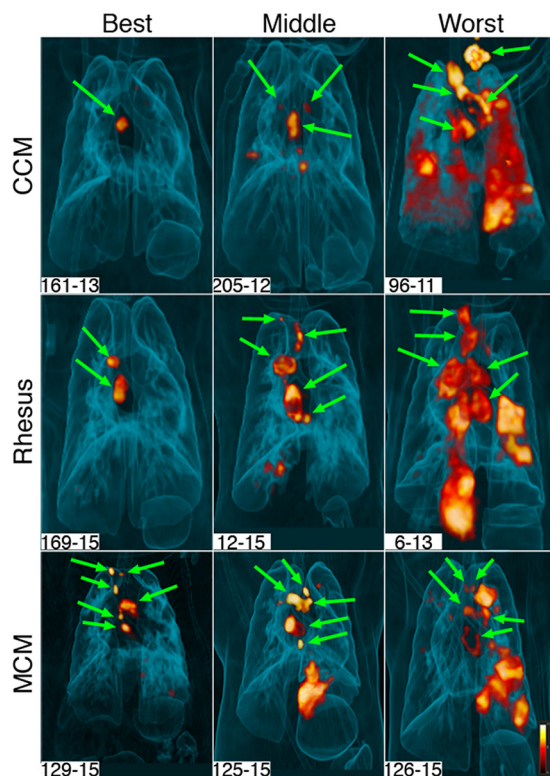


FIG 1 Range of inflammation among macaque species. Three-dimensional volume renderings of PET-CT scans of infected animals at 12 weeks postinfection are shown. Animals in all three species have a wide range of lung inflammation, ranging from minimal (represented as “Best”) to extensive (represented as “Worst”). Green arrows show thoracic lymph nodes. All other pathology seen on these scans is within the lungs. All of the animals depicted here have granulomas, although small lesions are not visible on these images.

only coughing was a significantly different objective clinical sign, based on the collection of clinical data and observations, only 39% of rhesus macaques reached the humane euthanasia endpoint prior to the planned necropsy date compared to only 15% for CCM ($P = 0.0926$ by Fisher’s exact test).

Although only two of the six MCM had reported cough and a separate two MCM had a positive GA or BAL fluid sample at >60 days p.i., four did not reach the planned endpoint of 5 months postinfection. Surprisingly, the ESR was relatively low in all these animals throughout infection, irrespective of TB severity.

PET-CT imaging distinguishes the extent of disease in macaques. Serial PET-CT imaging using [^{18}F]fluorodeoxyglucose (FDG) as a PET probe is a relatively noninvasive approach that provides insight into the infection process over time. We have used this imaging technology in macaques to assess early events in *M. tuberculosis* infection, reactivation kinetics, responses to drug treatment and vaccination, and, where possible, compared with human imaging data (16, 26, 29, 30, 32, 33). Here, we performed serial PET-CT imaging on each macaque in this study to assess similarities and differences among species during infection. The wide variability in disease severity between and among species is reflected by these PET-CT scans. Representative three-dimensional (3-D) scans of the best, middle, and worst monkey (in terms of disease severity) of each macaque species at 12 weeks are shown in Fig. 1. The green arrows show thoracic lymph nodes (LNs), and the remainder of PET activity is in the lung parenchyma. These images demonstrate that at least some animals of all three macaque species were capable of controlling the extent of TB disease over 12 weeks, while at least some animals of all three species exhibited poor control over the same time period.

To determine more precisely the differences in TB progression rate between the three macaque populations, we employed quantitative analyses of our imaging data.

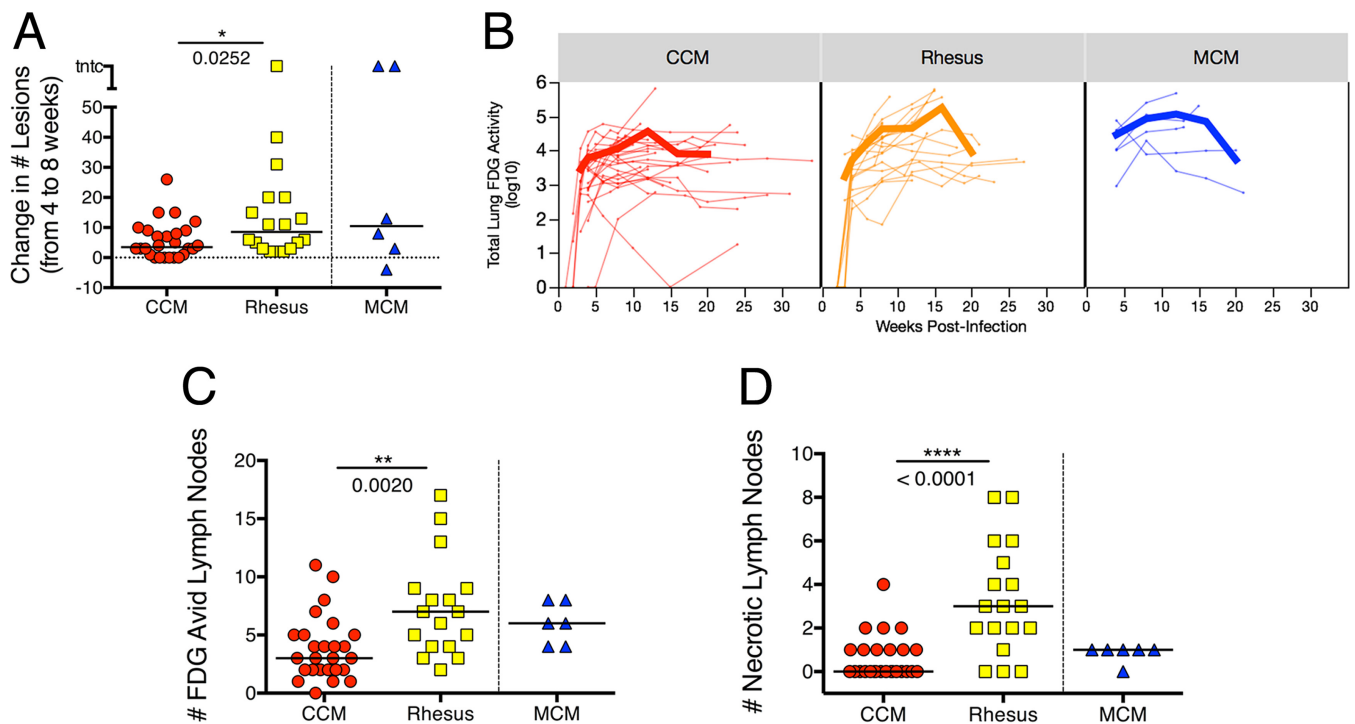


FIG 2 Comparison of scan outcomes across species. (A) Change in numbers of granulomas from 4 to 8 weeks postinfection, as a measure of dissemination. (B) Total lung inflammation over time as measured by FDG avidity on PET scan. Each thin line represents an individual animal, and the thick lines represent means for species. On average, there is a higher rate of increase in inflammation in rhesus macaques than in Chinese cynomolgus macaques (CCM). The later time points are for fewer animals, and the animals necropsied after 4 months postinfection tend to have less severe disease, which is why the average total FDG avidity decreases. (C) Number of FDG-avid (standard uptake value with muscle ratio [SUV_R] > 5) thoracic lymph nodes, as measured by PET-CT immediately prior to necropsy. (D) Number of necrotic lymph nodes observed on PET-CT scan. When a lymph node becomes necrotic, it appears donut-shaped on the scan, where the SUV values are higher around the circumference of the structure. These data are from PET-CT scans immediately prior to necropsy. In panels A, C, and D, each symbol represents the value for one animal, and short lines represent medians of the groups. Mann-Whitney test was used to compare CCM and rhesus macaque groups; Mauritian cynomolgus macaques (MCM) are not included in statistical comparisons.

Dissemination of infection can be defined as the formation of new granulomas after initial establishment of infection, and early dissemination is an indicator of eventual development of active disease (31). Dissemination can be monitored by PET-CT (31, 33). Here we assessed the formation of new granulomas that appeared between 4 and 8 weeks postinfection in each macaque (Fig. 2A), using axial orientation for each scan (31). Four weeks postinfection is the most reliable time point for identifying initial granulomas, since by that time, all initial granulomas are large enough (≥ 1 mm) to be seen by CT. Counting the increase in the number of granulomas between 4 and 8 weeks in each monkey indicated that rhesus macaques have significantly more *M. tuberculosis* dissemination than CCM do (median numbers of new granulomas of 8.5 in rhesus macaques and 3.5 for CCM; $P = 0.025$), although there is considerable variability among animals from each species. MCM have a wide range of dissemination as well, although one of the six MCM had four granulomas that resolved prior to the 8-week scan.

We have used total FDG avidity in lungs to assess overall inflammation and shown that it loosely correlates with lung bacterial burden following drug treatment in CCM (30). In this study, we found a wide range of total lung FDG avidity over the course of infection in both CCM and rhesus macaques (Fig. 2B), reflecting the heterogenous nature of *M. tuberculosis* infection in macaques. In particular, there were several CCM with low total FDG avidity ($< 1,000$ cumulative standard uptake value [SUV]) after 12 weeks of infection, while very few rhesus macaques showed low FDG avidity. Most MCM had relatively high FDG avidity throughout infection. A linear mixed-effects (LME) regression model was used to compare the lung inflammation [$\log_{10}(\text{inflammation} + 1)$] between species over time (see Table S2 and Fig. S1 in the supplemental material). This analysis confirmed that lung inflammation over the course of infection varies

between species (interaction term of species \times time; $P < 0.0001$). Assessing total FDG avidity over time in each species revealed that while there was similar lung inflammation between rhesus macaques and CCM at intermediate (e.g., 8-week) time points, rhesus macaques tend to start with lower inflammation that increases at a higher rate over the course of infection (Fig. 2B). At 3 weeks postinfection, rhesus macaques have less lung inflammation than CCM ($P = 0.0215$), while at 12 and 16 weeks postinfection, rhesus macaques tend to have more lung inflammation ($P = 0.0997$ and $P = 0.0566$, respectively) (Fig. S2).

PET-CT also provides the ability to track thoracic lymph node inflammation, which is related to *M. tuberculosis* infection of those lymph nodes (unpublished data). There are several thoracic lymph nodes in macaques, and the number of lymph nodes that are visible or recoverable can vary by monkey. Lymph nodes can be difficult to discern by PET-CT unless they are enlarged or FDG avid. It is also possible to visualize extensive necrosis of lymph nodes, which occurs as granulomas within the lymph node destroy the normal lymph node architecture. This appears as a lymph node with a “ring” of FDG avidity as a result of FDG being excluded from the center of the lymph node due to necrosis (Fig. S3). We determined the number of FDG-avid thoracic lymph nodes in each animal at necropsy, regardless of the time of necropsy (Fig. 2C). There were significantly more FDG-avid thoracic lymph nodes in rhesus macaques than in CCM (median value of 7 for rhesus versus 3 for CCM; $P = 0.002$), and MCM were more similar to rhesus macaques (median value of 6). Extensive lymph node necrosis was seen primarily in rhesus macaques; the median number of LNs with extensive necrosis in rhesus macaques was significantly higher than in the CCM (median number of necrotic lymph nodes in rhesus macaques of 3 versus 0 for CCM; $P < 0.0001$), while MCM were in between the two species (median = 1) (Fig. 2D).

More gross pathology is present in rhesus macaques than in CCM. PET-CT imaging indicated that infection progressed more rapidly and resulted in more extensive lung and lymph node disease in rhesus macaques than in CCM. MCM were similar to rhesus macaques in terms of both lung inflammation and lymph node involvement by PET-CT imaging. We then performed quantitative assessments of the macaques at necropsy. Gross pathology scores were determined using a modified version of our previously published scoring system (6) (see Text S1 in the supplemental material for the revised scoring system). This was revised to expand the dynamic scoring range for lymph node disease in order to capture better the extensive lymph node involvement we noted in rhesus macaques. This revised scoring system was used to assess all macaques in this study. Although there was a range of disease in all species, the median pathology scores were significantly higher in rhesus macaques than in CCM (median pathology scores of 33.5 for CCM and 59.5 for rhesus macaques; $P = 0.0005$), while MCM pathology scores were similar to rhesus macaque scores (median pathology score for MCM of 62) (Fig. 3A). Separating lung pathology (Fig. 3B) and lymph node pathology (Fig. 3C) scores showed that rhesus macaques have significantly higher lung ($P = 0.0059$) and lymph node ($P = 0.0099$) pathology compared to CCM (median lung scores of 10.5 for CCM and 25.5 for rhesus macaques; median lymph node scores of 17.5 for CCM and 23 for rhesus macaques). These data support the PET-CT data that rhesus macaques develop more progressive TB disease following low-dose challenge than CCM do and that MCM are more similar to rhesus macaques in terms of disease development (median lung score of 33 for MCM; median lymph node score of 21.5 for MCM).

Although TB is typically considered a lung infection, dissemination can occur outside the lungs to any organ, both in humans and in macaques. Liver and spleen granulomas are the most commonly seen extrapulmonary manifestation, but kidney granulomas, paravertebral and paracostal abscesses, and pancreatic lymph node involvement were also observed in this study. The extrapulmonary score takes into account the pathology for each organ outside the lung and the number of extrapulmonary samples, including granulomas, that were positive for growth of *M. tuberculosis*. Surprisingly, some gran-

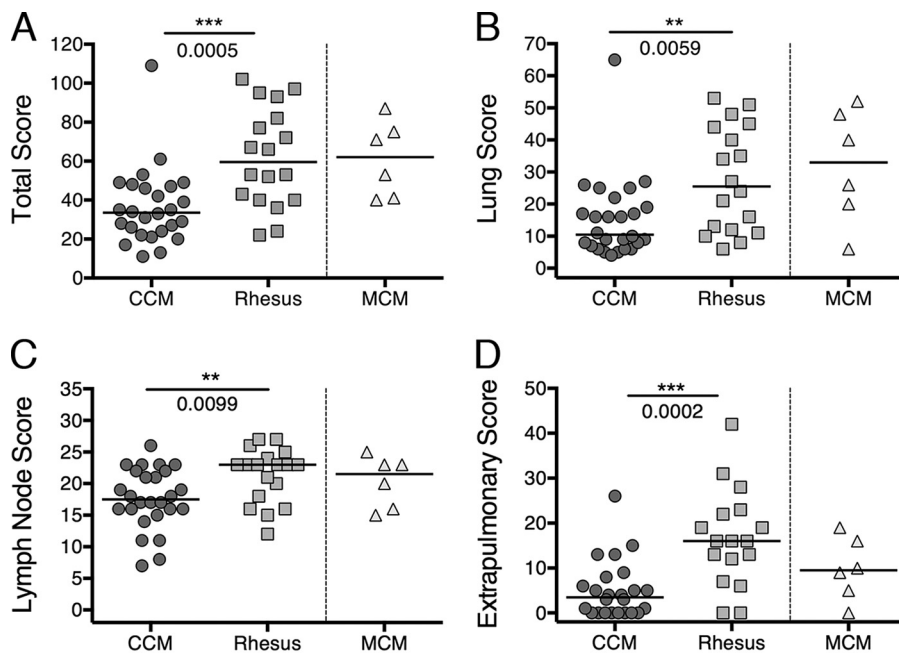


FIG 3 Gross pathology scores across species. (A) Total pathology score (aggregate of lung, lymph nodes, and extrapulmonary pathology). The highest possible score is 139. (B) Lung pathology score. The highest possible score is 74. (C) Lymph node score. The highest possible score is 28. (D) Extrapulmonary score. The extrapulmonary score combines the number of CFU-positive samples of sites outside the thoracic cavity and the extrapulmonary portion of the pathology score for each animal. Each symbol represents the value for one animal, and the short lines represent medians for groups. The Mann-Whitney test was used to compare CCM and rhesus groups; MCM were not included in statistical analyses due to the small number of animals.

ulomas observed grossly in the liver or spleen do not yield *M. tuberculosis* CFU (colony-forming units), similar to a subset of granulomas in the lungs (26, 32). Using this extrapulmonary scoring system, rhesus macaques had significantly higher extrapulmonary scores than CCM did (median extrapulmonary scores of 16.0 for rhesus macaques and 3.5 for CCM; $P = 0.0002$); 15/26 (58%) of CCM had extrapulmonary involvement compared to 16/18 (89%) rhesus macaques and 5/6 (83%) of MCM (Fig. 3D).

Bacterial burden following low-dose infection is higher in rhesus macaques than in Chinese cynomolgus macaques. Bacterial burden has been the gold standard to assess disease in animal models of TB. Although past studies have reported bacterial burden by various means, here we calculate a very close approximation of actual bacterial burden in lungs and thoracic lymph nodes. This is done by excising each lung granuloma or other lesion (e.g., consolidations or TB pneumonia) and plating each specimen individually and calculating the true bacterial burden of each lesion. Numerous random samples of grossly uninvolved lung specimens from each of the seven lobes were also plated, and the number of total bacteria was extrapolated from the weight of each entire lung lobe. In this way, the true bacterial burden for the lungs can be determined. Finally, all thoracic lymph nodes found from each animal, regardless of whether a granuloma was apparent, were individually plated, and the bacterial burden for each node was determined. The median numbers of thoracic lymph nodes recovered at necropsy were 8 (range, 7 to 13) for CCM, 11 (range, 6 to 14) for rhesus macaques, and 10 (range, 9 to 12) for MCM. The sum of all of these samples provided true thoracic bacterial burden (lung plus lymph nodes). This method is similar to that used in our previous publication on reactivation of latent *M. tuberculosis* infection (32).

The range of infection outcomes for CCM observed clinically and by PET-CT was reflected in the bacterial burden (Fig. 4A). Although the median thoracic bacterial burden (lung plus thoracic lymph nodes) for CCM was 37,893 CFU, the range was from 731 to 3×10^7 CFU. The CCM with the highest bacterial burden had miliary TB, with a

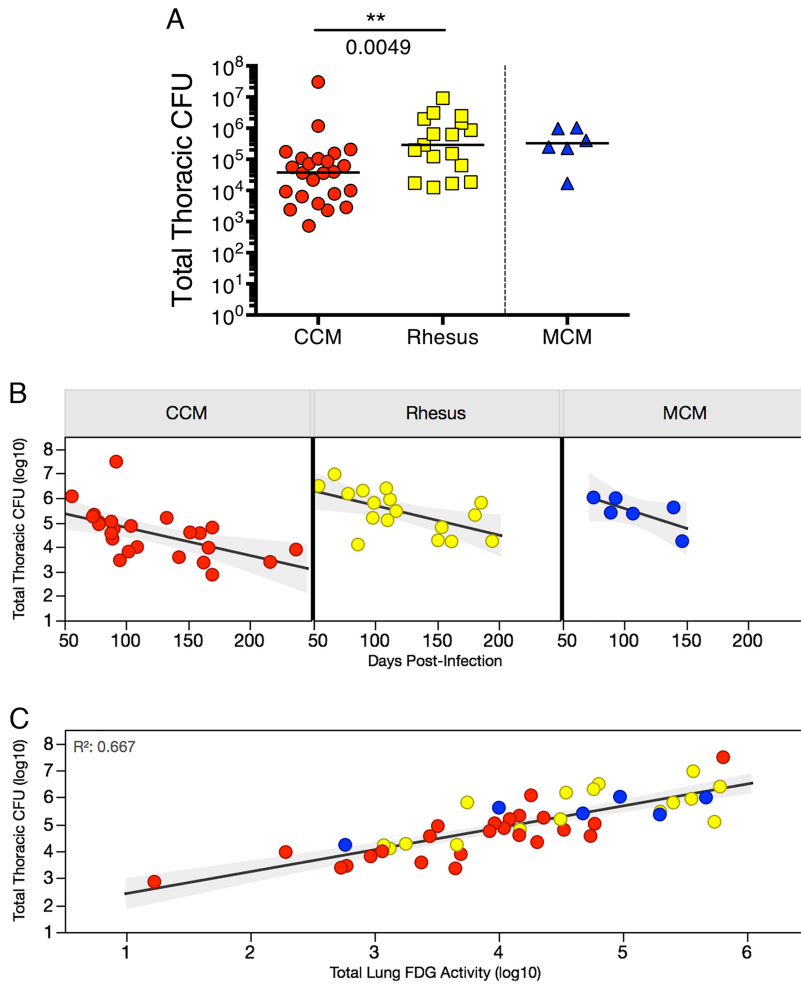


FIG 4 Total thoracic bacterial burden is higher in rhesus compared to CCM. (A) Total thoracic CFU (lung plus lymph nodes) across species. The unpaired *t* test (on log₁₀ transformation of total CFU + 1) was used to compare CCM and rhesus macaques. The lines represent medians for groups. (B) Total thoracic CFU at time of necropsy (days postinfection) by species. Linear regression analysis was performed, and the following statistics were found: for CCM, *R*² = 0.306 and *P* = 0.0051; for rhesus macaques, *R*² = 0.335 and *P* = 0.0150; for MCM, *R*² = 0.515 and *P* = 0.1085. (C) Lung inflammation (FDG avidity) is correlated with total thoracic CFU at the time of necropsy. Linear regression was performed on log₁₀ transformation (of value + 1) (on both variables) for all animals in study: *R*² = 0.667 and *P* < 0.0001. Each symbol represents the value for an individual animal in all panels. Red symbols represent CCM, yellow symbols represent rhesus macaques, and blue symbols represent MCM.

bacterial burden more than 25-fold higher than that of the CCM with the next highest bacterial burden. In contrast, the rhesus macaques assessed in this study had a smaller range of bacterial burdens (12,491 to 9.2×10^6) and a significantly higher median thoracic bacterial burden (median, 290,835) than CCM (*P* = 0.0049). The thoracic bacterial burden of MCM was similar to that of rhesus macaques with a median of 329,083 CFU (range, 17,111 to 1.04×10^6 CFU). Although as a group, rhesus macaques have higher bacterial burdens than CCM, it should be noted that outcome in all species is quite variable, and there is a large range of bacterial burdens in all three species assessed here. However, 9 of the 26 CCM had a total thoracic bacterial burden of <10,000 CFU, while all 18 rhesus macaques (and all 6 MCM) had bacterial burdens of >10,000 CFU. Thus, there is a subset of CCM that naturally control infection to a relatively low level that is not seen in the rhesus macaques or MCM in this study.

Total thoracic CFU tends to decrease over the course of infection (Fig. 4B), with bacterial killing in granulomas beginning after 4 weeks of infection (26). We performed

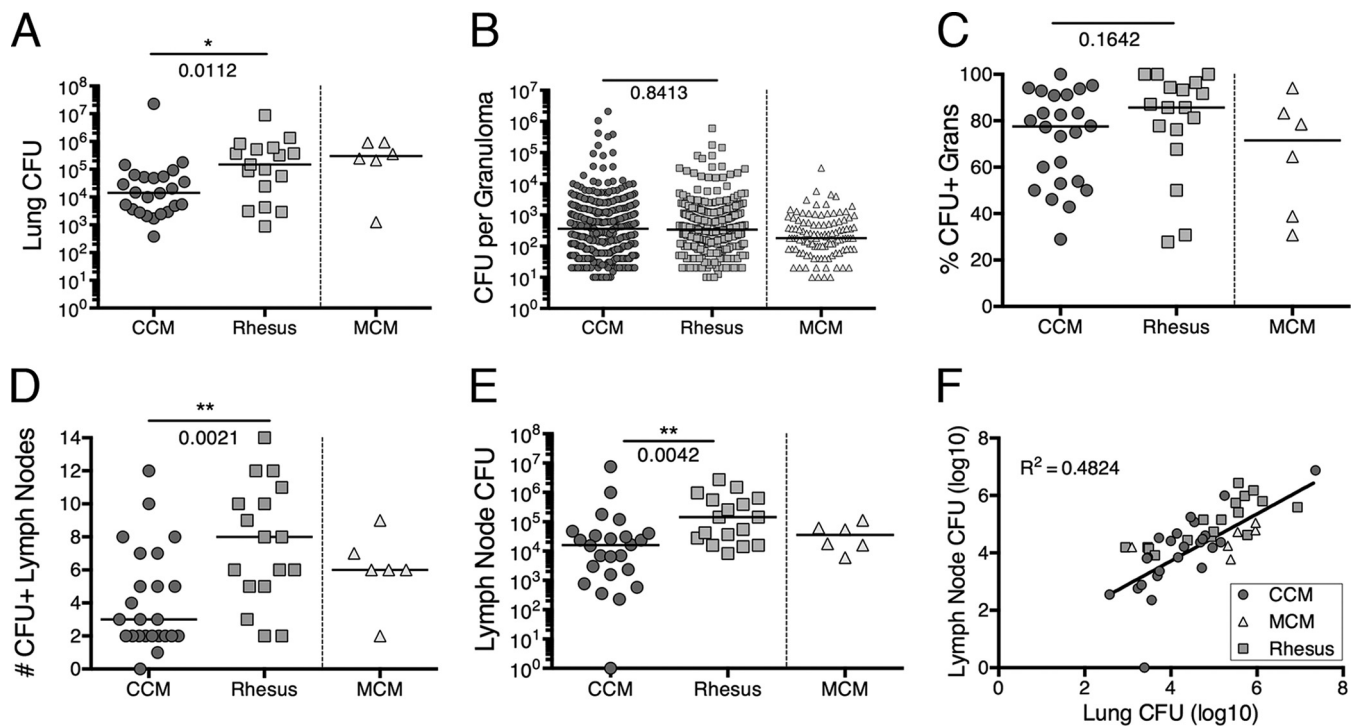


FIG 5 Bacterial burdens of lungs and lymph nodes. (A) Lung bacterial burden represents the total CFU within the lungs. This measurement includes granulomas, clusters, consolidations, and any bacteria grown from grossly uninvolved lung tissue. (B) Number of CFU per granuloma or cluster of granulomas. The numbers of individual granuloma CFU are similar in CCM and rhesus; this excludes sterile (CFU-negative) granulomas. All CFU+ granulomas from each animal are represented in this graph. (C) Fraction of granulomas that are CFU+ in each species. The Mann-Whitney test was used to compare CCM and rhesus macaques. (D) Number of CFU+ lymph nodes per animal. (E) The total lymph node bacterial burden is the sum of all CFU+ lymph nodes in each animal. Each symbol represents the value for an individual macaque in panels A, C, D, and E. Lines represent medians for groups. The Mann-Whitney test was used to compare CCM and rhesus macaques in panels A, B, and C. The unpaired *t* test was used to compare CCM and rhesus macaques in panels D and E (on log₁₀ transformation of lymph node CFU + 1). MCM were not included in statistical analyses. (F) Correlation between lymph node and lung CFU. All macaque species are shown. Linear regression was performed ($P < 0.0001$).

an ANCOVA (analysis of covariance) of log₁₀(total CFU + 1) to assess the linear relationship between the number of CFU and days postinfection (i.e., at necropsy) to determine whether this relationship differed between CCM and rhesus macaques (Table S3). This analysis indicates that CFU decreases significantly ($b = -0.01$; standard error [SE] = 0.003; $P = 0.0003$) and while total CFU of CCM is significantly lower than that of rhesus macaques ($b = -0.44$; SE = 0.128; $P = 0.0014$), CFU decreases at the same rate for both species (interaction term $P = 0.9110$) (Table S3). Although we demonstrated previously that there is increased sterilization of granulomas over the course of infection (26), this decrease in total CFU over time is likely also influenced by the earlier necropsy of animals with more severe disease. The total FDG avidity in lungs correlated with total thoracic (lung plus lymph node) CFU at necropsy in all species ($R^2 = 0.667$; $P < 0.0001$) (Fig. 4C). Thus, FDG avidity by PET scanning can be used as an *in vivo* surrogate for actual thoracic bacterial burden.

The total thoracic bacterial burden is comprised of lung and lymph node components. The median lung bacterial burden in rhesus macaques was approximately 10-fold higher than the median burden in CCM ($P = 0.0112$), although the ranges of lung CFU were similar for all three species, including MCM (Fig. 5A). Since each granuloma is individually plated, the number of CFU per granuloma can be compared between species. There was no significant difference in the median number of CFUs per granuloma for rhesus macaques and CCM (Fig. 5B); this analysis includes clusters (one to three granulomas) but excludes sterile granulomas and more-complex pathologies such as consolidations. This likely reflects that most granulomas can contain only a certain bacterial load threshold (i.e., carrying capacity) before evolving into more-complex pathologies, consistent with our previous study (26). An analysis of the

percentage of granulomas positive for CFU (CFU+) in each species reveals a wide range, from 28 to 100 (Fig. 5C), with a higher frequency of CFU+ granulomas observed in the first 3 months of infection (Fig. 54), as shown previously in CCM (26). All three species appear capable of completely killing bacteria within a subset of granulomas.

We calculated the number of CFU+ thoracic lymph nodes in each macaque (Fig. 5D). As expected from the PET-CT data (Fig. 2C), rhesus macaques had significantly more CFU+ thoracic lymph nodes than CCM did (median numbers of CFU+ thoracic lymph nodes and 8 for rhesus macaques and 3 for CCM; $P = 0.0021$). Although bacterial burden per involved lymph node was only slightly higher in rhesus macaques (median bacterial burdens per involved lymph node of 2,321 for CCM and 4,891 for rhesus macaques; $P = 0.0264$) (Fig. 55), the overall LN bacterial burden in rhesus macaques was nearly 10-fold higher than in CCM ($P = 0.0042$) (Fig. 5E), due to the higher number of involved lymph nodes in rhesus macaques. There is a positive correlation between total lung and total LN CFU when all macaques in this study were analyzed. Rhesus macaque LN CFU appears to be higher than expected (above the fit line), and MCM LN CFU appears to be lower than expected (below the fit line), whereas CCM are well dispersed around the line (Fig. 5F). This indicates a relationship between the bacterial burden in the lungs and LNs of an individual animal.

DISCUSSION

Although there are several animal models used in *M. tuberculosis* research, NHPs are the mostly closely related to humans, both genetically and with respect to *M. tuberculosis* infection outcome and pathology. Macaques are the most commonly used NHP species in TB research. Our goal for this study was to provide qualitative and quantitative comparisons between macaque species to identify similarities and differences to help researchers choose the most appropriate model system for different types of experiments or to help interpret published data. While comparative studies have been done previously, the current study uses several different methodologies and large sample sizes (except for MCM) to provide a more comprehensive and quantitative comparison between the species most commonly used for TB research.

The data presented here show that macaques exhibit a range of outcomes following low-dose *M. tuberculosis* infection. However, CCM develop fewer clinical signs of disease compared to rhesus macaques, and most CCM reached the end of the study without reaching the humane euthanasia endpoint. PET-CT analysis indicates that CCM had significantly reduced dissemination of granulomas, a slower increase in lung inflammation, and fewer FDG-avid or necrotic thoracic lymph nodes compared to rhesus macaques. These clinical and imaging parameters were confirmed at necropsy when gross pathology scores for both the lungs and lymph nodes were significantly higher in rhesus macaques than in CCM. In our experience, the more extensive lymph node involvement in rhesus macaques more often results in clinical signs of severe disease, with lymph nodes impinging on airways and occasionally causing collapse of lung lobes or erosion of lymph nodes into airways. Although this can occur in CCM, it is much less frequent. Enlarged thoracic lymph nodes may also increase the frequency of coughing. Extrapulmonary involvement was also higher in rhesus macaques than in CCM, reflecting increased dissemination outside the lungs. In published studies using low-dose aerosol challenge in small groups of animals and different analysis metrics, CCM were also less susceptible to progressive disease than rhesus macaques (19).

MCM are much less genetically diverse than standard cynomolgus macaques, and thus hold great potential for immunologic studies. They have greatly restricted major histocompatibility complex (MHC) alleles, which allows construction of tetramers that can recognize pathogen-specific T cells, and have been used to study simian immunodeficiency virus (SIV) pathogenesis and host response (38–42). Our PET-CT and necropsy data support the conclusion that MCM are similar to rhesus macaques in terms of *M. tuberculosis* dissemination, lung inflammation, and number of FDG-avid lymph nodes but more similar to CCM in terms of lymph node necrosis as determined by PET-CT. At necropsy, gross pathology of lung and lymph nodes in the MCM was

substantial, similar to rhesus macaques. A recent study of aerosolized *M. tuberculosis* infection of MCM also supports the idea that these macaques are very susceptible to progressive TB disease (21), although that study indicated that MCM were more susceptible than rhesus macaques. A limitation of our current study is that only six MCM were available for analysis, and thus, statistical analyses could not be performed reliably as there were substantially higher numbers of CCM and rhesus macaques.

Bacterial burden in this study was determined by harvesting and plating each granuloma and other pathologies and all thoracic lymph nodes as well as multiple samples from grossly uninvolved areas of each lung lobe. Thus, a much more accurate bacterial burden could be calculated for each animal, rather than reporting the numbers of CFU per gram or extrapolating from simply random sampling. By these methods, it becomes clear what a large range of bacterial burdens are found after experimental *M. tuberculosis* infection in all macaque species. However, the total bacterial burden is often lower than that seen in small-animal models, such as the mouse, where the lung bacterial burden typically ranges from 10^5 to 10^6 CFU in C57BL/6 mice, the most commonly used mouse strain (43). Macaques with bacterial burdens similar to the bacterial burdens of mice generally have extensive TB disease with abundant inflammation, while mice with similar bacterial burdens can survive for many months with little to no outward sign of disease. This may reflect differences in lung inflammation in primates and smaller animals and could be an area of important investigation.

This study also demonstrates the utility of PET-CT imaging for monitoring infection dynamics as well as for estimating bacterial burden, as we show that total FDG avidity in the lungs is a reasonable surrogate for total thoracic bacterial burden in all three species studied. Using the full range of imaging, pathology, and microbiologic parameters, rhesus macaques are more susceptible to developing progressive disease than CCM are. However, it should be noted that the full range of outcomes is observed in CCM, from well-contained infection (LTBI) to aggressive TB disease. In contrast, we did not find convincing evidence of LTBI in rhesus macaques after low-dose challenge with virulent *M. tuberculosis*. These data provide important information for researchers to better understand the various macaque models used for tuberculosis research. In addition, these data provide the opportunity to more properly power NHP studies based on concrete endpoints. For vaccine studies, for example, the more susceptible rhesus macaque may be more difficult to fully protect. However, since most unvaccinated monkeys progress to active TB rather quickly, fewer monkeys may be necessary to see a major vaccine effect. In contrast, cynomolgus macaques of Chinese origin demonstrate the full range of infection outcomes, similar to humans. However, since approximately half of cynomolgus macaques will control the infection quite well without vaccination, sample sizes in vaccine studies with these animals are necessarily larger. These macaques may be more appropriate for studies of TB pathogenesis and host responses, including LTBI and reactivation TB. Finally, the MCM, while quite susceptible to TB disease, provide unique opportunities for careful study of host immune responses, given their restricted MHC repertoire and the potential for development of tetramer reagents for the study of *M. tuberculosis*-specific T cells, and are likely to be useful models for vaccine testing.

MATERIALS AND METHODS

Animals. Cynomolgus macaques ($n = 26$) were obtained from Valley Biosystems (West Sacramento, CA). These cynomolgus macaques were purposely bred in China (i.e., Chinese origin) (Chinese cynomolgus macaques [CCM]) and quarantined domestically at Valley Biosystems (West Sacramento, CA). Chinese origin rhesus macaques ($n = 18$) were purchased from PrimGen (Hines, IL) and Covance Inc. (Princeton, NJ). Cynomolgus macaques ($n = 6$) were obtained from Bioculture, Ltd. (Mauritian cynomolgus macaques [MCM]) and quarantined domestically at Buckshire Corporation (Perkasie, PA). Upon arrival at the University of Pittsburgh, all animals were quarantined for 1 to 3 months, confirmed to be negative for intestinal parasites, simian immunodeficiency virus, simian T lymphotropic virus, and simian retrovirus, and were screened for preexisting *M. tuberculosis* infection by tuberculin skin testing and/or enzyme-linked immunosorbent spot assays (ELISPOs). All animals reported here were control animals (i.e., no drug, vaccine, or immunologic interventions) enrolled in studies in the Flynn, Scanga, and Lin labora-

tories between 2011 and 2017. All animals and infection date, dose, and necropsy date are listed in Table S1 in the supplemental material. Some of the data reported here on a subset of the macaques have been reported in previous publications (as control animals for certain studies), as noted in Table S1 (31, 32, 44). These studies were conducted in an AAALAC-approved biosafety level 3 (BSL-3) facility within the Regional Biocontainment Laboratory at the University of Pittsburgh. All studies and animal procedures were approved by the University of Pittsburgh Institutional Animal Care and Use Committee, and the University of Pittsburgh Division of Laboratory Animal Resources is AAALAC approved.

Infection. Macaques were infected with *M. tuberculosis* strain Erdman (diluted in 2 ml of sterile saline) via bronchoscopic instillation into a lower lung lobe, as previously described (6). This Erdman strain is well characterized (26, 45) and has been used for all our published studies in macaques (e.g., 5, 6). The infection dose was estimated by plating an aliquot of inoculum on 7H11 plates and enumerating CFU after 21 days of incubation. Infection doses for the animals in this study ranged from 3 to 20 CFU for CCM, 7 to 18 CFU for rhesus macaques, and 3 to 41 CFU for MCM. Infection was confirmed by PET-CT scan, tuberculin skin testing, and ELISPOts for *M. tuberculosis*-specific antigens as previously described (6, 31).

Clinical and microbiologic monitoring and humane euthanasia endpoints. We used clinical criteria to identify signs of TB disease as previously published (5, 6). Macaques were monitored monthly for erythrocyte sedimentation rate (ESR) and weight and given physical exams. General appearance, appetite, coughing, lethargy, and respiratory pattern were noted daily. Gastric aspirate (GA) samples and bronchoalveolar lavage (BAL) fluid samples were obtained monthly as previously described (6) and plated for *M. tuberculosis* growth. Humane euthanasia endpoints include weight loss (which is rare), anorexia, prolonged cough, sustained increased respiratory rate or effort, and significant behavioral changes. PET-CT data were also used, in conjunction with clinical data, to determine whether an animal had reached humane euthanasia endpoint.

PET-CT. Animals were imaged using positron emission tomography (PET) with 2-deoxy-2-¹⁸F-D-deoxyglucose (FDG) (microPET Focus 220 preclinical PET scanner; Siemens Molecular Solutions, Knoxville, TN) and computed tomography (CT) (Neurologica Corp., Danvers, MA) as previously described (30). All scans were viewed and analyzed using OsiriX (Pixmeo, Geneva, Switzerland), a DICOM (digital imaging and communications in medicine) viewer. Individual granulomas were identified on scans and counted at 4 weeks postinfection and 8 weeks postinfection. The maximum standard uptake value (SUV) of each mediastinal lymph node was identified and recorded as described in reference 46. Lymph nodes with SUV_r (SUV with muscle ratio) greater than or equal to 5 were then counted (46). Total lung FDG activity is a cumulative measurement of SUV values, where the SUV of every "hot" voxel (all voxels with a SUV greater than 2.3) is added up within the lung cavity (46).

Necropsy and gross pathology scoring. For necropsy, macaques are maximally bled and humanely euthanized using sodium pentobarbital after being deeply sedated with ketamine. The necropsies are performed by trained pathologists or physicians. Gross pathology scoring, a quantitative measure of TB disease, is based on the careful analysis of numbers and sizes of granulomas or other pathologies in each lung lobe (on surface and parenchyma), size and degree of granuloma involvement within each mediastinal lymph node, and number and size of granulomas within extrapulmonary sites (e.g., liver, spleen). At necropsy, lesions seen on PET-CT scans were matched to lesions at necropsy. The previously published (6) gross necropsy scoring sheet was updated to reflect the larger number of thoracic lymph nodes involved that is often found in rhesus macaques and is provided in Text S1 in the supplemental material.

The pathology score can be separated into three components: lung, lymph nodes (LNs), and extrapulmonary. The extrapulmonary portion of the pathology score can range from 0 to 37 and takes into account the number of sites involved on the diaphragm, body wall, liver, spleen, or other abdominal viscera. For each site, the number of visible granulomas and size of the largest granuloma contribute to the score (minimum score of 0 and maximum score of 10). In order for an organ to score a full "10" points, a miliary pattern must be seen with the largest visible granuloma measuring >4 mm. In this set of macaques, 2 to 20 extrapulmonary samples were taken to plate for CFU for each animal. Unlike the lung and LN scoring, the number of culture-positive extrapulmonary samples in each macaque was combined with the extrapulmonary pathology score to represent the total extrapulmonary score.

Bacterial burden analysis at necropsy. All individual lung granulomas, complex pathologies, and thoracic and some peripheral (axial and inguinal) lymph nodes were divided in half (or for very small granulomas, kept whole), weighed, and homogenized in at least 2 ml of phosphate-buffered saline (PBS) either by pushing the tissue sample through a 0.70- μ m cell strainer for small granulomas or using a MediMachine system (BD Biosciences) for larger samples. The remaining portion was submitted for histology. Each lung lobe was dissected to identify and harvest all granulomas and pathologies (limit of detection for granulomas was ~1 mm by PET-CT scan as well as by visual inspection). The remaining lobe was cut into 2- to 3-mm pieces, and approximately half was weighed and used for determining bacterial burden, and the other half was fixed in formalin for histology. The lung lobes were individually homogenized. Plating samples for CFU was performed on 7H11 plates. The plates were incubated at 37°C for 3 weeks, and colonies were counted. The actual bacterial burden of each sample was calculated. Total lung and lymph node bacterial burden is the sum of all samples taken from the thoracic cavity.

Statistics. Statistical comparisons were made only between rhesus macaques and Chinese cynomolgus macaques. Mauritian macaques are shown only for visual reference. For normal data, the *t* test was used to compare the two groups, and for nonnormal data, the Mann-Whitney test was used. Fisher's exact test was used to analyze any categorical data. GraphPad Prism version 6.0 h for Mac OS X (GraphPad Software, La Jolla, CA, USA) was used for all *t* tests and Mann-Whitney tests, and JMP Pro version 12.1.0 64-bit (SAS Institute Inc., Cary, NC) was used for any other statistics reported.

A linear mixed-effects (LME) regression model was utilized to compare the lung inflammation [$\log_{10}(\text{inflammation} + 1)$] as determined by PET scans between species over time. The fixed effects included in this model were species (CCM and rhesus macaques), time postinfection (as a classification variable), and the interaction term species \times time. Assuming that the slope and intercept of lung inflammation varies over time for individual monkeys, a random intercept and slope model (weeks represented as a continuous variable) was used with unbounded variance components. It was assumed that errors are independent. Random-effects covariance parameter estimates and fixed-effects tests are shown in Table S2. Least-squares means estimates with 95% confidence intervals over time are shown in Fig. S1. Lung inflammation (FDG avidity) of the species was compared at each time point postinfection using *t* tests, and *P* values without multiple-comparison adjustments were reported (Fig. S2).

To assess differences in total bacterial burden (CFU) at necropsy over time between rhesus macaques and CCM, an analysis of covariance (ANCOVA) was utilized on $\log_{10}(\text{total CFU} + 1)$. In this model, species was included as a nominal fixed factor and the number of days to necropsy was used as a continuous covariate. Parameter estimates and least-squares mean estimates are shown in Table S3.

SUPPLEMENTAL MATERIAL

Supplemental material for this article may be found at <https://doi.org/10.1128/IAI.00505-17>.

SUPPLEMENTAL FILE 1, PDF file, 3.3 MB.

ACKNOWLEDGMENTS

We acknowledge the outstanding technical and intellectual contributions of all members of the Flynn, Lin, and Scanga laboratories, as well as the pathology expertise of Edwin Klein. We thank Chelsea Chedrick for preparation of figures. We are also grateful to Patricia Darrah, Robert Seder, and Mario Roederer at the NIH Vaccine Research Center for donation of the rhesus macaques used in this study.

These studies were supported by grants from the NIH (HL110811, AI118195, and AI094745 [J.L.F.], AI111815 [C.A.S.], AI111871 [P.L.L.], T32 AI0089443 [A.M.C.], and T32 AI060525 [R.M.D.]), AERAS Foundation, and Bill and Melinda Gates Foundation.

REFERENCES

- World Health Organization. 2016. Global tuberculosis report 2016. World Health Organization, Geneva, Switzerland.
- Colditz GA, Brewer TF, Berkey CS, Wilson ME, Burdick E, Fineberg HV, Mosteller F. 1994. Efficacy of BCG vaccine in the prevention of tuberculosis. Meta-analysis of the published literature. *JAMA* 271:698–702.
- Flynn JL, Tsenova L, Izzo A, Kaplan G. 2008. Experimental animal models of tuberculosis, p 389–417. *In* Kaufmann SHE, van Helden P, Rubin E, Britton WJ (ed), *Handbook of tuberculosis: immunology and cell biology*, vol 2. Wiley-Blackwell, Hoboken, NJ.
- McShane H, Williams A. 2014. A review of preclinical animal models utilised for TB vaccine evaluation in the context of recent human efficacy data. *Tuberculosis (Edinb)* 94:105–110. <https://doi.org/10.1016/j.tube.2013.11.003>.
- Capuano SV III, Croix DA, Pawar S, Zinovic A, Myers A, Lin PL, Bissel S, Fuhrman C, Klein E, Flynn JL. 2003. Experimental Mycobacterium tuberculosis infection of cynomolgus macaques closely resembles the various manifestations of human M. tuberculosis infection. *Infect Immun* 71:5831–5844. <https://doi.org/10.1128/IAI.71.10.5831-5844.2003>.
- Lin PL, Rodgers M, Smith L, Bigbee M, Myers A, Bigbee C, Chiosea I, Capuano SV, Fuhrman C, Klein E, Flynn JL. 2009. Quantitative comparison of active and latent tuberculosis in the cynomolgus macaque model. *Infect Immun* 77:4631–4642. <https://doi.org/10.1128/IAI.00592-09>.
- Flynn JL, Klein E. 2011. Pulmonary tuberculosis in monkeys, p 83–106. *In* Leong FJ, Darois V, Dick T (ed), *A color atlas of comparative pathology of pulmonary tuberculosis*. Taylor & Francis Publishers, Boca Raton, FL.
- Scanga CA, Flynn JL. 2014. Modeling tuberculosis in nonhuman primates. *Cold Spring Harb Perspect Med* 4:a018564. <https://doi.org/10.1101/cshperspect.a018564>.
- Barclay WR, Busey WM, Dalgard DW, Good RC, Janick RW, Kasik JE, Ribi E, Ulrich CE, Wolinsky E. 1973. Protection of monkeys against airborne tuberculosis by aerosol vaccination with Bacillus Calmette-Guerin. *Am Rev Respir Dis* 107:351–358.
- Barclay WR, Anacker RL, Brehmer W, Leif W, Ribi E. 1970. Aerosol-induced tuberculosis in subhuman primates and the course of the disease after intravenous BCG vaccination. *Infect Immun* 2:574–582.
- Walsh GP, Tan EV, dela Cruz EC, Abalos RM, Villahermosa LG, Young LJ, Cellona RV, Nazareno JB, Horwitz MA. 1996. The Philippine cynomolgus monkey (*Macaca fascicularis*) provides a new nonhuman primate model of tuberculosis that resembles human disease. *Nat Med* 2:430–436. <https://doi.org/10.1038/nm0496-430>.
- Rizvi N, Rao NA, Hussain M. 2000. Yield of gastric lavage and bronchial wash in pulmonary tuberculosis. *Int J Tuberc Lung Dis* 4:147–151.
- Al-Marri MR, Kirkpatrick MB. 2000. Erythrocyte sedimentation rate in childhood tuberculosis: is it still worthwhile? *Int J Tuberc Lung Dis* 4:237–239.
- Lin PL, Myers A, Smith L, Bigbee C, Bigbee M, Fuhrman C, Grieser H, Chiosea I, Voitenek NN, Capuano SV, Klein E, Flynn JL. 2010. Tumor necrosis factor neutralization results in disseminated disease in acute and latent Mycobacterium tuberculosis infection with normal granuloma structure in a cynomolgus macaque model. *Arthritis Rheum* 62:340–350. <https://doi.org/10.1002/art.27536>.
- Lin PL, Rutledge T, Green AM, Bigbee M, Fuhrman C, Klein E, Flynn JL. 2012. CD4 T cell depletion exacerbates acute Mycobacterium tuberculosis while reactivation of latent infection is dependent on severity of tissue depletion in cynomolgus macaques. *AIDS Res Hum Retroviruses* 28:1693–1702. <https://doi.org/10.1089/aid.2012.0028>.
- Diedrich CR, Mattila JT, Klein E, Janssen C, Phuah J, Sturgeon TJ, Montelaro RC, Lin PL, Flynn JL. 2010. Reactivation of latent tuberculosis in cynomolgus macaques infected with SIV is associated with early peripheral T cell depletion and not virus load. *PLoS One* 5:e9611. <https://doi.org/10.1371/journal.pone.0009611>.
- Verreck FA, Vervenne RA, Kondova I, van Kralingen KW, Remarque EJ, Braskamp G, van der Werff NM, Kersbergen A, Ottenhoff TH, Heidt PJ, Gilbert SC, Gicquel B, Hill AV, Martin C, McShane H, Thomas AW. 2009. MVA.85A boosting of BCG and an attenuated, *phoP* deficient M. tuberculosis vaccine both show protective efficacy against tuberculosis in rhesus macaques. *PLoS One* 4:e5264. <https://doi.org/10.1371/journal.pone.0005264>.
- Verreck FAW, Tchilian EZ, Vervenne RAW, Sombroek CC, Kondova I, Eissen OA, Sommandas V, van der Werff NM, Verschoor E, Braskamp G,

- Bakker J, Langermans JAM, Heidt PJ, Ottenhoff THM, van Kralingen KW, Thomas AW, Beverley PCL, Kocken CHM. 2017. Variable BCG efficacy in rhesus populations: pulmonary BCG provides protection where standard intra-dermal vaccination fails. *Tuberculosis (Edinb)* 104:46–57. <https://doi.org/10.1016/j.tube.2017.02.003>.
19. Sharpe S, White A, Gleeson F, McIntyre A, Smyth D, Clark S, Sarfas C, Laddy D, Rayner E, Hall G, Williams A, Dennis M. 2015. Ultra low dose aerosol challenge with *Mycobacterium tuberculosis* leads to divergent outcomes in rhesus and cynomolgus macaques. *Tuberculosis (Edinb)* 96:1–12. <https://doi.org/10.1016/j.tube.2015.10.004>.
 20. Sharpe SA, Eschelbach E, Basaraba RJ, Gleeson F, Hall GA, McIntyre A, Williams A, Kraft SL, Clark S, Gooch K, Hatch G, Orme IM, Marsh PD, Dennis MJ. 2009. Determination of lesion volume by MRI and stereology in a macaque model of tuberculosis. *Tuberculosis (Edinb)* 89:405–416. <https://doi.org/10.1016/j.tube.2009.09.002>.
 21. Sharpe SA, White AD, Sibley L, Gleeson F, Hall GA, Basaraba RJ, McIntyre A, Clark SO, Gooch K, Marsh PD, Williams A, Dennis MJ. 2017. An aerosol challenge model of tuberculosis in Mauritian cynomolgus macaques. *PLoS One* 12:e0171906. <https://doi.org/10.1371/journal.pone.0171906>.
 22. Langermans JA, Andersen P, van Soelingen D, Vervenne IM, Frost PA, van der Laan T, van Pinxteren LA, van den Hombergh J, Kroon S, Peekel I, Florquin S, Thomas AW. 2001. Divergent effect of bacillus Calmette-Guerin (BCG) vaccination on *Mycobacterium tuberculosis* infection in highly related macaque species: implications for primate models in tuberculosis vaccine research. *Proc Natl Acad Sci U S A* 98:11497–11502. <https://doi.org/10.1073/pnas.201404898>.
 23. Gormus BJ, Blanchard JL, Alvarez XH, Didier PJ. 2004. Evidence for a rhesus monkey model of asymptomatic tuberculosis. *J Med Primatol* 33:134–145. <https://doi.org/10.1111/j.1600-0684.2004.00062.x>.
 24. Foreman TW, Mehra S, LoBato DN, Malek A, Alvarez X, Golden NA, Bucsan AN, Didier PJ, Doyle-Meyers LA, Russell-Lodrigue KE, Roy CJ, Blanchard J, Kuroda MJ, Lackner AA, Chan J, Khader SA, Jacobs WR, Jr, Kaushal D. 2016. CD4+ T-cell-independent mechanisms suppress reactivation of latent tuberculosis in a macaque model of HIV coinfection. *Proc Natl Acad Sci U S A* 113:E5636–E5644. <https://doi.org/10.1073/pnas.1611987113>.
 25. Sibley L, Dennis M, Sarfas C, White A, Clark S, Gleeson F, McIntyre A, Rayner E, Pearson G, Williams A, Marsh P, Sharpe S. 2016. Route of delivery to the airway influences the distribution of pulmonary disease but not the outcome of *Mycobacterium tuberculosis* infection in rhesus macaques. *Tuberculosis (Edinb)* 96:141–149. <https://doi.org/10.1016/j.tube.2015.11.004>.
 26. Lin PL, Ford CB, Coleman MT, Myers AJ, Gawande R, Ioerger T, Sacchetti J, Fortune SM, Flynn JL. 2014. Sterilization of granulomas is common in active and latent tuberculosis despite within-host variability in bacterial killing. *Nat Med* 20:75–79. <https://doi.org/10.1038/nm.3412>.
 27. Cadena AM, Fortune SM, Flynn JL. 2017. Heterogeneity in tuberculosis. *Nat Rev Immunol* 17:691–702. <https://doi.org/10.1038/nri.2017.69>.
 28. Lewinsohn DM, Tydeman IS, Frieder M, Grotzke JE, Lines RA, Ahmed S, Prongay KD, Primack SL, Colgin LM, Lewis AD, Lewinsohn DA. 2006. High resolution radiographic and fine immunologic definition of TB disease progression in the rhesus macaque. *Microbes Infect* 8:2587–2598. <https://doi.org/10.1016/j.micinf.2006.07.007>.
 29. Lin PL, Coleman T, Carney JP, Lopresti BJ, Tomko J, Fillmore D, Dartois V, Scanga C, Frye LJ, Janssen C, Klein E, Barry CE, III, Flynn JL. 2013. Radiologic responses in cynomolgus macaques for assessing tuberculosis chemotherapy regimens. *Antimicrob Agents Chemother* 57:4237–4244. <https://doi.org/10.1128/AAC.00277-13>.
 30. Coleman MT, Chen RY, Lee M, Lin PL, Dodd LE, Maiello P, Via LE, Kim Y, Marriner G, Dartois V, Scanga C, Janssen C, Wang J, Klein E, Cho SN, Barry CE, III, Flynn JL. 2014. PET/CT imaging reveals a therapeutic response to oxazolidinones in macaques and humans with tuberculosis. *Sci Transl Med* 6:265ra167. <https://doi.org/10.1126/scitranslmed.3009500>.
 31. Coleman MT, Maiello P, Tomko J, Frye LJ, Fillmore D, Janssen C, Klein E, Lin PL. 2014. Early changes by ¹⁸F-fluorodeoxyglucose positron emission tomography coregistered with computed tomography predict outcome after *Mycobacterium tuberculosis* infection in cynomolgus macaques. *Infect Immun* 82:2400–2404. <https://doi.org/10.1128/IAI.01599-13>.
 32. Lin PL, Maiello P, Gideon HP, Coleman MT, Cadena AM, Rodgers MA, Gregg R, O'Malley M, Tomko J, Fillmore D, Frye LJ, Rutledge T, DiFazio RM, Janssen C, Klein E, Andersen PL, Fortune SM, Flynn JL. 2016. PET CT identifies reactivation risk in cynomolgus macaques with latent *M. tuberculosis*. *PLoS Pathog* 12:e1005739. <https://doi.org/10.1371/journal.ppat.1005739>.
 33. Martin CJ, Cadena AM, Leung VW, Lin PL, Maiello P, Hicks N, Chase MR, Flynn JL, Fortune SM. 2017. Digitally barcoding *Mycobacterium tuberculosis* reveals in vivo infection dynamics in the macaque model of tuberculosis. *mBio* 8:e00312-17. <https://doi.org/10.1128/mBio.00312-17>.
 34. Yan G, Zhang G, Fang X, Zhang Y, Li C, Ling F, Cooper DN, Li Q, Li Y, van Gool AJ, Du H, Chen J, Chen R, Zhang P, Huang Z, Thompson JR, Meng Y, Bai Y, Wang J, Zhuo M, Wang T, Huang Y, Wei L, Li J, Wang Z, Hu H, Yang P, Le L, Stenson PD, Li B, Liu X, Ball EV, An N, Huang Q, Zhang Y, Fan W, Zhang X, Li Y, Wang W, Katze MG, Su B, Nielsen R, Yang H, Wang J, Wang X, Wang J. 2011. Genome sequencing and comparison of two nonhuman primate animal models, the cynomolgus and Chinese rhesus macaques. *Nat Biotechnol* 29:1019–1023. <https://doi.org/10.1038/nbt.1992>.
 35. Mothe BR, Lindestam Arlehamn CS, Dow C, Dillon MB, Wiseman RW, Bohn P, Karl J, Golden NA, Gilpin T, Foreman TW, Rodgers MA, Mehra S, Scriba TJ, Flynn JL, Kaushal D, O'Connor DH, Sette A. 2015. The TB-specific CD4+ T cell immune repertoire in both cynomolgus and rhesus macaques largely overlap with humans. *Tuberculosis (Edinb)* 95:722–735. <https://doi.org/10.1016/j.tube.2015.07.005>.
 36. Kanthaswamy S, Ng J, Satkoski Trask J, George DA, Kou AJ, Hoffman LN, Doherty TB, Houghton P, Smith DG. 2013. The genetic composition of populations of cynomolgus macaques (*Macaca fascicularis*) used in biomedical research. *J Med Primatol* 42:120–131. <https://doi.org/10.1111/jmp.12043>.
 37. Javed S, Marsay L, Wareham A, Lewandowski KS, Williams A, Dennis MJ, Sharpe S, Vipond R, Silman N, Ball G, Kempell KE. 2016. Temporal expression of peripheral blood leukocyte biomarkers in a *Macaca fascicularis* infection model of tuberculosis: comparison with human datasets and analysis with parametric/non-parametric tools for improved diagnostic biomarker identification. *PLoS One* 11:e0154320. <https://doi.org/10.1371/journal.pone.0154320>.
 38. O'Connor SL, Becker EA, Weinfurter JT, Chin EN, Budde ML, Gostick E, Correll M, Gleicher M, Hughes AL, Price DA, Friedrich TC, O'Connor DH. 2012. Conditional CD8+ T cell escape during acute simian immunodeficiency virus infection. *J Virol* 86:605–609. <https://doi.org/10.1128/JVI.05511-11>.
 39. O'Connor SL, Blasky AJ, Pendley CJ, Becker EA, Wiseman RW, Karl JA, Hughes AL, O'Connor DH. 2007. Comprehensive characterization of MHC class II haplotypes in Mauritian cynomolgus macaques. *Immunogenetics* 59:449–462. <https://doi.org/10.1007/s00251-007-0209-7>.
 40. O'Connor SL, Lhost JJ, Becker EA, Detmer AM, Johnson RC, Macnair CE, Wiseman RW, Karl JA, Greene JM, Burwitz BJ, Bimber BN, Lank SM, Tuscher JJ, Mee ET, Rose NJ, Desrosiers RC, Hughes AL, Friedrich TC, Carrington M, O'Connor DH. 2010. MHC heterozygote advantage in simian immunodeficiency virus-infected Mauritian cynomolgus macaques. *Sci Transl Med* 2:22ra18. <https://doi.org/10.1126/scitranslmed.3000524>.
 41. Wiseman RW, Karl JA, Bimber BN, O'Leary CE, Lank SM, Tuscher JJ, Detmer AM, Bouffard P, Levenkova N, Turcotte CL, Szekeres E, Jr, Wright C, Harkins T, O'Connor DH. 2009. Major histocompatibility complex genotyping with massively parallel pyrosequencing. *Nat Med* 15:1322–1326. <https://doi.org/10.1038/nm.2038>.
 42. Wiseman RW, Wojcechowskyj JA, Greene JM, Blasky AJ, Gopon T, Soma T, Friedrich TC, O'Connor SL, O'Connor DH. 2007. Simian immunodeficiency virus SIVmac239 infection of major histocompatibility complex-identical cynomolgus macaques from Mauritius. *J Virol* 81:349–361. <https://doi.org/10.1128/JVI.01841-06>.
 43. Cooper AM, Khader SA. 2008. The role of cytokines in the initiation, expansion, and control of cellular immunity to tuberculosis. *Immunol Rev* 226:191–204. <https://doi.org/10.1111/j.1600-065X.2008.00702.x>.
 44. Phuah J, Wong EA, Gideon HP, Maiello P, Coleman MT, Hendricks MR, Ruden R, Cirrincione LR, Chan J, Lin PL, Flynn JL. 2016. Effects of B cell depletion on early *Mycobacterium tuberculosis* infection in cynomolgus macaques. *Infect Immun* 84:1301–1311. <https://doi.org/10.1128/IAI.00083-16>.
 45. Ford CB, Lin PL, Chase MR, Shah RR, Iartchouk O, Galagan J, Mohaideen N, Ioerger TR, Sacchetti J, Lipsitch M, Flynn JL, Fortune SM. 2011. Use of whole genome sequencing to estimate the mutation rate of *Mycobacterium tuberculosis* during latent infection. *Nat Genet* 43:482–486. <https://doi.org/10.1038/ng.811>.
 46. White AG, Maiello P, Coleman MT, Tomko JA, Frye LJ, Scanga CA, Lin PL, Flynn JL. 2017. Analysis of ¹⁸F-FDG PET/CT imaging as a tool for studying *Mycobacterium tuberculosis* infection and treatment in non-human primates. *J Vis Exp* 2017(127):e56375. <https://doi.org/10.3791/56375>.